AIP Journal of Applied Physics

Electrical and optical properties of Ta-Si-N thin films deposited by reactive magnetron sputtering

D. Oezer, G. Ramírez, S. E. Rodil, and R. Sanjinés

Citation: J. Appl. Phys. **112**, 114302 (2012); doi: 10.1063/1.4766904
View online: http://dx.doi.org/10.1063/1.4766904
View Table of Contents: http://jap.aip.org/resource/1/JAPIAU/v112/i11
Published by the AIP Publishing LLC.

Additional information on J. Appl. Phys.

Journal Homepage: http://jap.aip.org/
Journal Information: http://jap.aip.org/about/about_the_journal
Top downloads: http://jap.aip.org/features/most_downloaded
Information for Authors: http://jap.aip.org/authors

ADVERTISEMENT

Downloaded 09 Aug 2013 to 132.248.12.226. This article is copyrighted as indicated in the abstract. Reuse of AIP content is subject to the terms at: http://jap.aip.org/about/rights_and_permissions

JOURNAL OF APPLIED PHYSICS **112**, 114302 (2012)

Electrical and optical properties of Ta-Si-N thin films deposited by reactive magnetron sputtering

D. Oezer,[1] G. Ramírez,[2] S. E. Rodil,[2] and R. Sanjinés[1]
[1]*Ecole Polytechnique Fédérale de Lausanne (EPFL), Institute of Condensed Matter Physics (ICMP), CH-1015 Lausanne, Switzerland*
[2]*Instituto de Investigaciones en Materiales, Universidad Nacional Autónoma de México, Circuito Exterior s/n, CU, México D.F. 04510, Mexico*

(Received 4 May 2012; accepted 24 October 2012; published online 3 December 2012)

The electrical and optical properties of $Ta_xSi_yN_z$ thin films deposited by reactive magnetron sputtering from individual Ta and Si targets were studied in order to investigate the effects of nitrogen and silicon contents on both properties and their correlation to the film microstructure. Three sets of fcc-$Ta_xSi_yN_z$ thin films were prepared: sub-stoichiometric $Ta_xSi_yN_{0.44}$, nearly stoichiometric $Ta_xSi_yN_{0.5}$, and over-stoichiometric $Ta_xSi_yN_{0.56}$. The optical properties were investigated by near-normal-incidence reflectivity and ellipsometric measurements in the optical energy range from 0.375 eV to 6.8 eV, while the d.c. electrical resistivity was measured in the van der Pauw configuration from 20 K to 300 K. The optical and electrical measurements were interpreted using the standard Drude-Lorentz model and the so-called grain boundary scattering model, respectively. The electronic properties were closely correlated with the compositional and structural modifications of the $Ta_xSi_yN_z$ films due to variations in the stoichiometry of the fcc-TaN_z system and the addition of Si atoms. According to the nitrogen and silicon contents, fcc-$Ta_xSi_yN_z$ films can exhibit room temperature resistivity values ranging from 10^2 $\mu\Omega$ cm to about 6×10^4 $\mu\Omega$ cm. The interpretation of the experimental temperature-dependent resistivity data within the Grain Boundary Scattering model, combined with the results from optical investigations, showed that the mean electron transmission probability G and the free carriers concentration, N, are the main parameters that control the transport properties of these films. The results indicated that the correlation between electrical and optical measurements with the chemical composition and the nanostructure of the $Ta_xSi_yN_z$ thin films provides a pertinent and consistent description of the evolution of the Ta-Si-N system from a solid solution to a nanocomposite material due to the addition of Si atoms. © *2012 American Institute of Physics*. [http://dx.doi.org/10.1063/1.4766904]

I. INTRODUCTION

Among the transition metal-based nitrides (Me-N), Ta-N have received a lot of interest in the last decades not only due to its high melting point, high hardness, and corrosion resistance but also because of its relevant electrical and optical properties.[1–3] Tantalum nitride Ta-N is considered as an important material for industrial applications. As thin films, Ta-N is easily integrated in microelectronic devices and commonly used as diffusion barrier in magnetoresistive random access memory and resistors, since it works as an excellent barrier against Cu diffusion, or as preferred barrier absorber material for EUV mask.[4–8] The Ta-N system exhibits many phases and stoichiometries, such as hexagonal (hcp) γ-Ta_2N, hexagonal θ-TaN, face centered cubic δ-TaN, tetragonal Ta_4N_5, and orthorhombic Ta_3N_5.[9,10] Regarding their electrical properties, tetragonal Ta_3N_5 has been reported as being a semiconductor[10,11] while the hexagonal Ta_2N exhibits metal-like conductivity[4] and fcc-TaN_z behaves like dirty metal with negative temperature coefficient of resistivity due to weak carrier localization.[12]

In order to further improve the performances and efficiency of microelectronic devices based on transition metal nitrides, nanocrystalline or amorphous ternary systems, such as Me-Si-N, forming highly stable compounds, have been also investigated.[13–30] By the addition of Si to binary MeN, the hardness, thermal stability and chemical inertness of the films can be considerably improved. The addition of Si leads to the formation of a nanocomposite (nanocrystallites of MeN + amorphous SiN_x) or a solid solution of a single-phased $Me_{1-x}Si_xN$ material.[13–16] In nanocomposite thin films (nc-MeN/a-SiN_x), the crystallite sizes are of the order of a few nanometers. Therefore, the grain surfaces and boundary regions play an important role regarding the physical properties. The position, thickness, and chemical composition of the amorphous SiN_x phase are crucial for the electrical properties.[17–20] Thin films based on TaSiN, NbSiN, and WSiN have been mainly investigated as diffusion barriers and electrodes for phase change random access memory (PRAM) devices. In particular, TaSiN films have been shown to exhibit good chemical and thermal stability up to 1300 K and electrical resistivity values ranging from about 3×10^2 $\mu\Omega$cm to 8×10^4 $\mu\Omega$cm.[21–30]

In the present paper, an extensive analysis of the electrical and optical properties of reactively magnetron-sputtered $Ta_xSi_yN_z$ thin films is reported. The aim of the paper is to investigate the effects of nitrogen and silicon contents on the electronic properties of these films. Special attention is paid

 © 2012 American Institute of Physics

Downloaded 09 Aug 2013 to 132.248.12.226. This article is copyrighted as indicated in the abstract. Reuse of AIP content is subject to the terms at: http://jap.aip.org/about/rights_and_permissions

to the composition of the fcc-TaN_z films and to the structural modifications of these films due to the addition of Si atoms. From the fundamental point of view, stoichiometric deviations, structural disorder (vacancies, substitutional, antisites, and interstitial atoms), and phase composition influence the physical properties of these materials. Furthermore, the knowledge of the relations between the microstructure and the electrical and optical properties of single- or two-phase nanocomposite thin films will lead to a better understanding of their functional properties.

II. EXPERIMENTAL

In order to investigate the effects of the chemical composition on the electrical and optical properties of TaSiN films, three different series of films were deposited using two different reactor chambers. Each magnetron sputtering system is equipped with two confocal planar magnetron sources positioned with their axis about 25° or 30° off the vertical and the substrate-target distance was fixed at 100 mm. The substrates were mounted on a rotary sample holder manipulator to insure film homogeneity. The deposition chamber is connected to a turbo molecular pump through an adaptive pressure controller valve, which allows fixing the final total pressure in the sputtering chamber. Mass flow regulators are fitted for controlling independently the sputtering Ar gas and the reactive gases. The targets diameters were 5 cm in both cases. Firstly, sub-stoichiometric $Ta_xSi_yN_z$ samples with $0.42 < z < 0.44$ (referred in the paper as $Ta_xSi_yN_{0.44}$ samples or series A) were deposited using individual Si (99.999 at. %) and Ta (99.95 at. %) targets. A high DC power of 400 W was applied to the Ta target while a variable RF power ranging from 60 to 340 W was applied to the Si target in order to change the Si content (C_{Si}) in the $Ta_xSi_yN_{0.44}$ films. Before the deposition of the films, the residual pressure in the sputtering chamber was typically lower than 10^{-4} Pa. The substrate temperature was kept constant at 380 °C (653 K), the total working pressure, $P_T = (P_{Ar} + P_{N2})$, was fixed at 0.4 Pa using a N_2/ Ar flow ratio of 6/14. The second and third film series (namely, series B and C) were deposited using individual Ta (99.95 at. %) and Si (99.999 at. %) targets in a mixed $(Ar + N_2)$ atmosphere. The residual pressure in the reactor chamber was typically less than 10^{-4} Pa. The power applied to the Ta target was 100 W, while the DC power on the Si target was varied between 0 and 60 W. During the deposition, the total pressure P_T and the substrate temperature T_s were kept constant at 0.5 Pa and 480 °C (753 K), respectively. The two series B and C of $Ta_xSi_yN_z$ samples were deposited using N_2/Ar flow ratios of 2/13 and N_2/Ar = 7/13, respectively, leading to nearly stoichiometric films with $0.49 \leq z \leq 0.51$ (referred as $Ta_xSi_yN_{0.5}$ films or series B) and over-stoichiometric films with $0.54 \leq z \leq 0.57$ (denoted as $Ta_xSi_yN_{0.56}$ films or series C).

For the resistivity measurements, the films were deposited onto highly resistive (>800 Ωcm) Si or on oxidized Si wafers while for optical measurements the substrates were polished Si(100) wafers. The film thickness was measured by profilometry (Tencor PH50), obtaining typically 0.8–1.2 μm for the series B and C and about 1.2 μm for the series A (Dektak 150). The chemical composition of the $Ta_xSi_yN_z$ films was obtained by electron probe microanalyses (EPMA) and XPS measurements. The XPS measurements were performed using a commercial VG Microtech Multilab ESCA 2000. The contaminant element was found to be oxygen (≤ 3 at. %). The crystallographic phase was determined by x-ray diffraction using monochromatized Cu Kα radiation. The crystallite sizes of the films were estimated from both grazing incidence at 4° (GI-XRD) and θ–2θ Bragg Brentano (BB-XRD) configuration measurements.

The electrical resistivity measurements of all samples were performed using the van der Pauw method in the temperature range between 20 K and 300 K.

The optical properties of the films of series A were investigated by ellipsometric measurements in the photon energy range of 1.5–5.0 eV using an Uvisel Jobin-Yvon DH10 ellipsometer (at 70° as incident angle) and the data analysis was performed using the DeltaPsi2 software, while series B and C were characterized using an Uvisel Jobin-Yvon and Alpha-SE-Woollam ellipsometers (1.3–3.3 eV).

The optical reflectivity was measured using wavelengths from 180 to 3300 nm (6.8–0.375 eV) on a Cary 500 spectrometer.

III. RESULTS

A. Structure and morphology

Under the given deposition conditions, all the $Ta_xSi_yN_z$ films crystallized in the fcc NaCl-structure and exhibit a pronounced columnar-like morphology with elongated crystallites in the growth direction, as could be observed by cross section scanning electron images (not shown), i.e., not titling was introduced due to the confocal magnetron configuration, must probably because the substrates were rotated during deposition. The films exhibited a (100) preferred orientation, without presence of other peaks and only peak width variations were observed for the three series. The BB-XRD pattern of over-stoichiometric $Ta_xSi_yN_{0.56}$ films is shown in Fig. 1(a) as an example. The average crystallite sizes, calculated from the BB-XRD patterns using the simple Scherrer's formula, are presented in Fig. 1(b) for the three series. The general trend is the decrease of the crystallite size as the Si content increases in the films, except in the case of series A where the crystallite size decreased initially but increased again when the Si content was above 6 at. %. The decrease of the crystallite size and loss of the columnar-like morphology with increasing the Si content could be attributed to the formation of a nanocomposite film as a consequence of the Si segregation towards the grain boundaries, covering the surface of the crystallite and hindering the crystal growth. The surface coverage by Si atoms, Si_{cov} can be estimated from the simple relation $Si_{\mathrm{cov}} = \left(\frac{z}{3a}\right)\left(\frac{C_{Si}-\alpha}{C_{Ta}+\alpha}\right)$ where z is the crystallite size, a is the lattice constant, C_{Si} and C_{Ta} are the Si and Ta contents, respectively, and α is the solubility limit of Si into the MeN.[16,18–20] Assuming $a = 0.433$ nm and a Si solubility $\alpha = 0$ (this is reasonable as the Si solubility was found to be negligible in high temperature deposited films by sputtering[19,20]), the estimated Si_{cov} values for the 3 types of films are shown in Fig. 1(c). The Si coverage increased

Downloaded 09 Aug 2013 to 132.248.12.226. This article is copyrighted as indicated in the abstract. Reuse of AIP content is subject to the terms at: http://jap.aip.org/about/rights_and_permissions

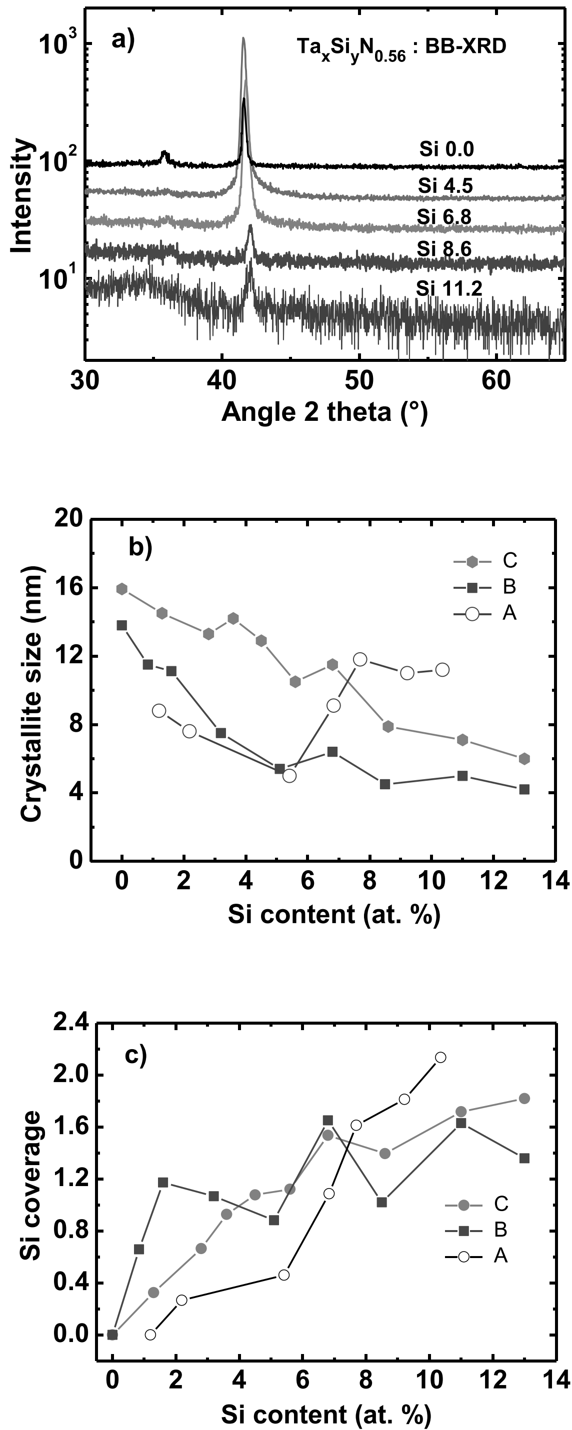

FIG. 1. (a) Typical X-Ray diffraction patterns of $Ta_xSi_yN_z$ thin films; $\theta-2\theta$ (BB-XRD) diffractograms of over-stoichiometric $Ta_xSi_yN_{0.56}$ films, (b) crystalline grain sizes calculated using the Scherrer equation for the three series, and (c) Si coverage estimated using the model described in Ref. 18.

B. Optical properties

1. Dielectric function and reflectivity

All the investigated $Ta_xSi_yN_z$ films were optically opaque, therefore ellipsometric measurements provided directly the complex dielectric function $\varepsilon(E) = \varepsilon_1(E) + i\varepsilon_2(E)$ of the films as well as the refractive index $n(E)$ and the extinction coefficient $k(E)$. The real and the imaginary parts of the complex permittivity function $\varepsilon(E) = \varepsilon_1(E) + i\varepsilon_2(E)$ of $Ta_xSi_yN_z$ films, deduced from ellipsometric measurement are shown in Figs. 2–4. In general, it might be observed that for TaN_z and $Ta_xSi_yN_z$ films with low Si content, the real part $\varepsilon_1(E)$ of the dielectric function exhibits a metallic like behavior. The position of the screened plasma energy, E_{ps}, which is defined as the energy for which ε_1 equals zero, changed insignificantly in comparison to those observed in pure TaN_z films. For both sub-stoichiometric and nearly stoichiometric films, the screened plasma energy for the lowest Si content lies about $E_{ps} = 4.0 \pm 0.1$ eV (see Figs. 2(a) and 3(a)), while for over-stoichiometric $TaN_{1.14}$ films, it lies at $E_{ps} = 3.3 \pm 0.1$ eV (see Fig. 4(a)). With increasing C_{Si} in the $Ta_xSi_yN_z$ films, the position of the screened plasma energy E_{ps} is progressively shifted towards lower energy values and a strong interband absorption arises below 2 eV, indicating a change from metallic to dielectric character. This behavior is well observed progressively as the Si content increased in the films. In the case of series B and C, the full coverage ($Si_{cov} = 1$) of the crystallite surface was found at about 4–5 Si at. % while in the series A, the full coverage seems to occur only above 7 at. %. It is worth noting that the $Si_{cov} = 1$ corresponding to one monolayer (1 ML) is equivalent in thickness to 2 ML of SiN_x between two adjacent TaN crystallites.

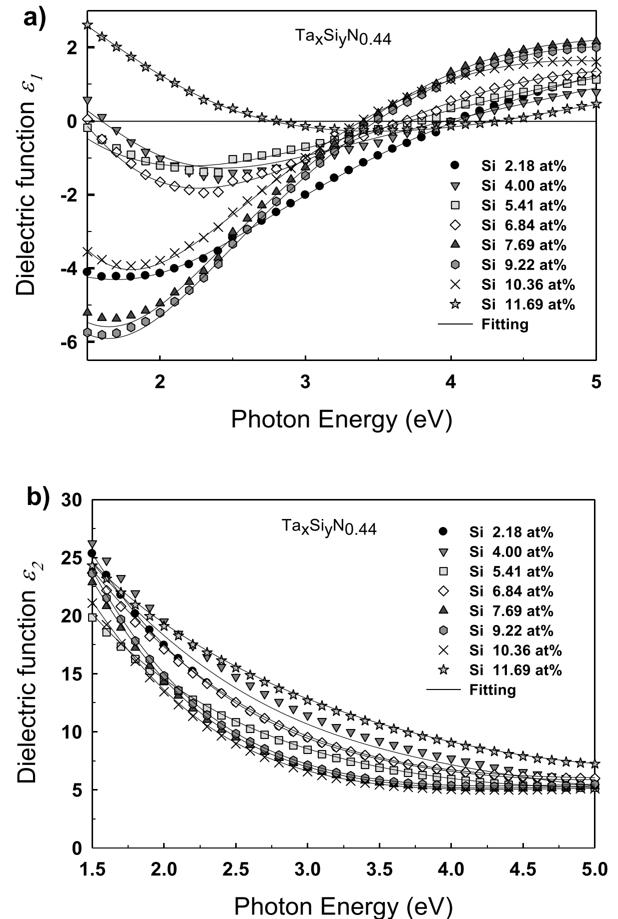

FIG. 2. (a) Real ε_1 and (b) imaginary ε_2 parts of the dielectric function of $Ta_xSi_yN_{0.44}$ thin films for selected Si content (in at. %) and fitted (solid lines) curves using the Drude-Lorentz model.

Downloaded 09 Aug 2013 to 132.248.12.226. This article is copyrighted as indicated in the abstract. Reuse of AIP content is subject to the terms at: http://jap.aip.org/about/rights_and_permissions

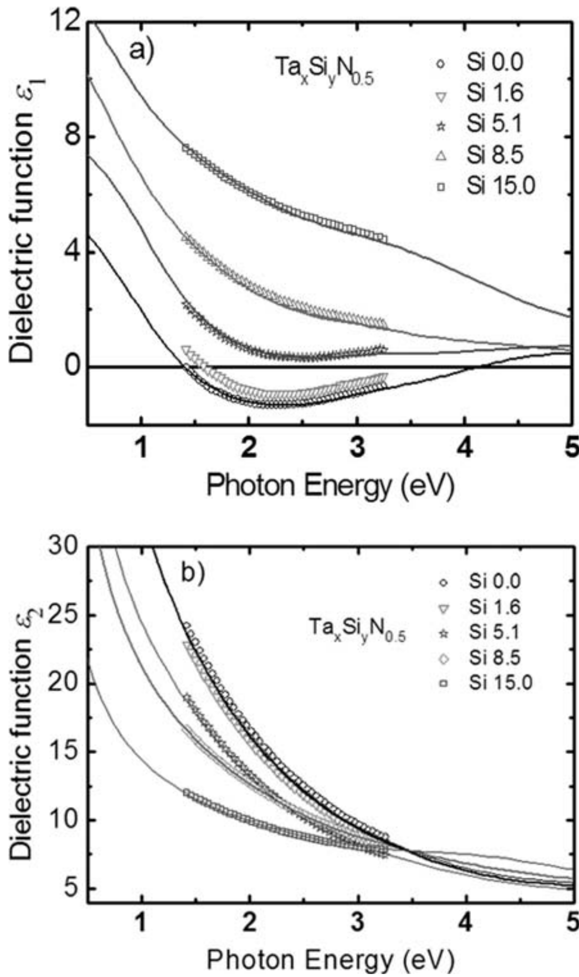

FIG. 3. (a) Real ε_1 and (b) imaginary ε_2 parts of the dielectric function of $Ta_xSi_yN_{0.5}$ thin films for selected Si content (in at. %) and fitted (solid lines) curves using the Drude-Lorentz model.

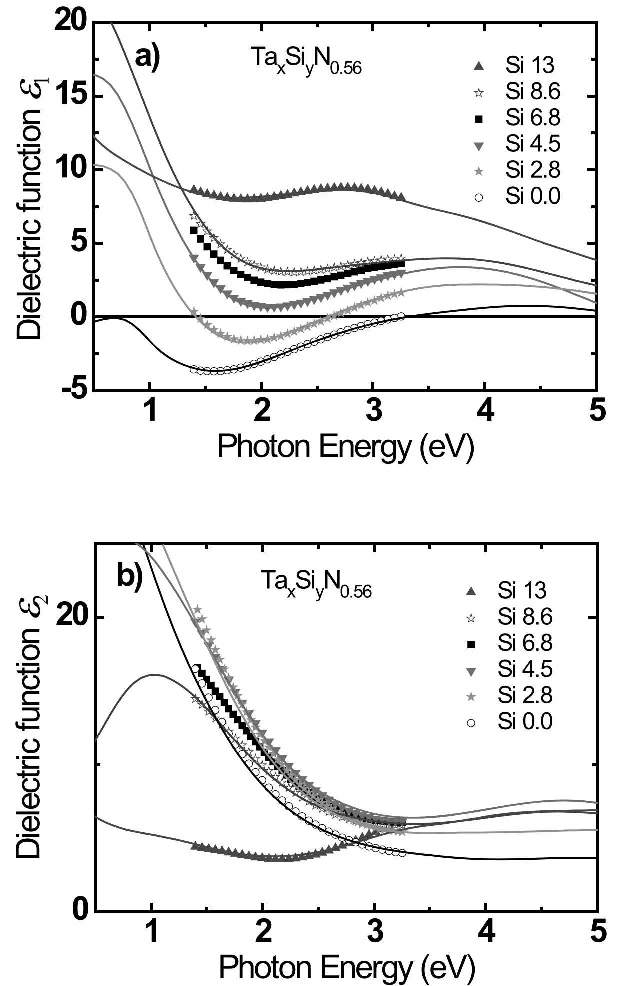

FIG. 4. (a) Real ε_1 and (b) imaginary ε_2 parts of the dielectric function of $Ta_xSi_yN_{0.56}$ thin films for selected Si content and fitted (solid lines) curves using the Drude-Lorentz model.

in the case of series B and C (Figs. 3(a) and 4(a)), but is less evident for the case of series A (Fig. 2(a)). For series B and C, the Si content required for the films to undergo a metal-to-dielectric-like transition is between 4 and 5 at. % (ε_1 does not cross by zero), while in the case of series A, E_{ps} remained in the energy range of 3–4 eV even for higher Si contents up to 11.7 at. %.

Fig. 5 shows the optical reflectivity spectra of selected $Ta_xSi_yN_z$ films as a function of the Si content. The reflectivity spectra of nearly stoichiometric films were characterized by a minimum reflectivity value of about 30% located at 5.5 eV. A reflectivity of about 70% at photon energy of 1.0 eV was observed in films containing a C_{Si} less than 3 at. %. At higher C_{Si} (> 3 at. %), the metallic-like reflectivity decreased as the Si content increased (Fig. 5(a)). Similar trends were observed in over-stoichiometric $Ta_xSi_yN_{0.56}$ films, but in this case the reflectivity minimum value of 22% was observed at 4.5 eV for pure $TaN_{1.14}$ films and was shifted to lower photon energies of about 2.0 eV as the Si content increased up to 13% (Fig. 5(b)). These films exhibit a brownish-yellow color. Regarding the sub-stoichiometric $Ta_xSi_yN_{0.44}$ films, optical reflectivity measurements were not relevant as the dielectric functions of these films exhibit a weak Si content dependence and remained metallic-like.

2. Drude-Lorentz model

The optical properties of most fcc MeN and MeSiN thin films[18,19,30–34] have been explained by modeling their dielectric functions considering contributions of intraband and interband transitions described by a Drude term and a set of Lorentz oscillators, respectively,

$$\varepsilon(E) = \varepsilon_\infty - \frac{E_p^2}{E^2 + i\Gamma_p E} + \sum_k \frac{f_k E_k^2}{E_k^2 - E^2 - i\Gamma_k E}, \qquad (1)$$

ε_∞ is a constant accounting for all higher-energy interband transitions that are not taken into account in the Lorentz terms. The Drude term is characterized by the plasma energy $E_p = \hbar\omega_p$ and the damping factor Γ_p, which are related to the electron density, N, and to the relaxation time, τ_p, of the free carriers: $N = \varepsilon_0 m_e \omega_p^2/e^2$, $\Gamma_p = \hbar/\tau_p$. The optical resistivity can be extracted from the relation $\rho_{op} = m_e/e^2 N\tau_p$. In the present study, four Lorentz oscillators located at about 1.5–2 eV, 3.5–4.0 eV, 5.0–6.0 eV, and 7.6 eV were introduced to account for interband transitions at the Γ and X points of the Brillouin zone. According to the band structure

Downloaded 09 Aug 2013 to 132.248.12.226. This article is copyrighted as indicated in the abstract. Reuse of AIP content is subject to the terms at: http://jap.aip.org/about/rights_and_permissions

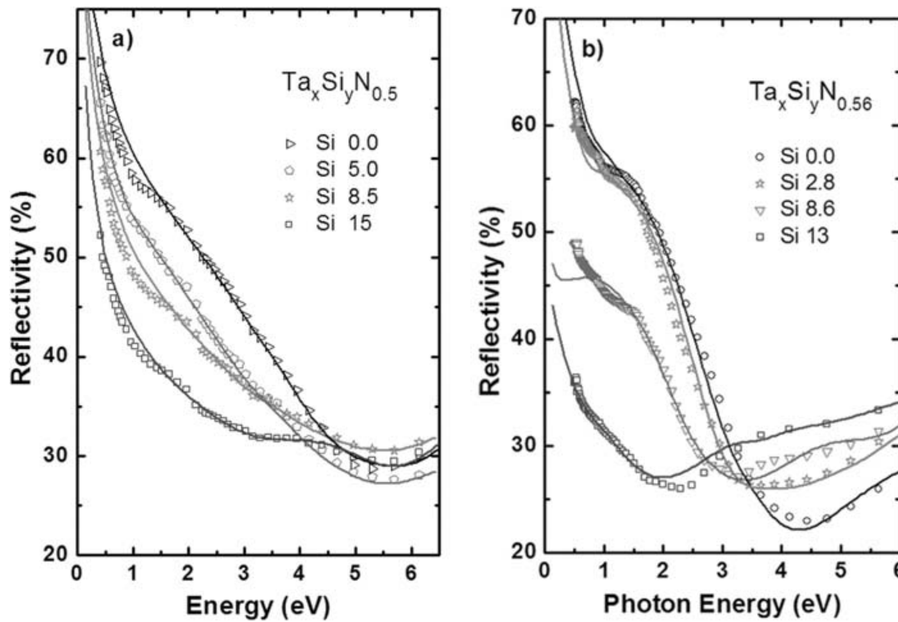

FIG. 5. Typical experimental and numerically calculated (solid lines) reflective spectra of: (a) near-stoichiometric $Ta_xSi_yN_{0.5}$ and (b) over-stoichiometric $Ta_xSi_yN_{0.56}$ thin films.

calculations reported for fcc TaN by Stampfl *et al.*,[35] the Fermi level lies at the bottom of a double degenerated 5 d band at the Γ point. In the Γ direction, the nearest upper and lower 5 d bands are located at about 2 eV above and at 2 eV and 4 eV below the Fermi level. Therefore, interband transitions are expected to occur at about 2.0 eV, 4.0 eV, and 5–6 eV. In the X direction, interband transitions are also likely to occur at slightly higher energies such as 6–8 eV.

The solid lines in Figs. 2 to 4 show the theoretical dielectric function curves calculated using relation (1) for all samples. The comparison between the experimental and theoretical curves is relatively good considering that modeling the free carrier density using the Drude-Lorentz approximation is not a trivial task since the separation of the free electron and interband contributions is difficult. However, confirmation of the models was obtained by calculating the reflectivity using the ellipsometric parameters and comparing the calculated R spectra with experimental measurements in the full photon energy range of (0.37–6.8) eV, as shown as the solid lines in Fig. 5 for series B and C. Though small differences were observed, the general trends between the experimental and theoretical curves were in relatively good agreement. Moreover, the validity of this interpretation procedure is confirmed by the good correlation found between the d.c. van der Pauw resistivity measurements and the calculated optical resistivities as discussed below.

The plasma energy, E_p, which impacts the free carrier concentration, was modified among the three series in different ways. In the case of nearly stoichiometric $Ta_xSi_yN_{0.5}$ (series B), the variations observed in the dielectric function as a function of the Si content (Fig. 3) can be simulated by varying $E_p = \hbar\omega_p$ between 9.8 eV and 4.2 eV and the damping factors, Γ_p, between 3 eV and 2 eV. These values gave rise to densities of free carries $N = (1.3-7) \times 10^{22}\,cm^{-3}$ and to relaxation times in the range of $\tau_p = (2.1 - 3.3) \times 10^{-16}$ s. The resulting optical resistivity values were $\rho_{op} = (240 - 840)$ $\mu\Omega$cm, in good agreement with those obtained from van der Pauw measurements (see below). Thus in the case of nearly stoichiometric TaN films, the addition of Si mainly leads to a progressive diminution of the density of the free carriers. This is graphically shown in Fig. 6, where the results from the three series are included. This behavior could be attributed to the decrease of the crystallite size, the introduction of high density of point defects (Ta vacancies, N antisites), and/or the formation of an insulating SiN_x thin layer surrounding the TaN crystallites.

In the case of nitrogen-deficient $Ta_xSi_yN_{0.44}$ films (series A), the situation was different. These films exhibited relatively high free carrier density values ($N = (3–8) \times 10^{22}\,cm^{-3}$), with τ_p values comparable to those of series B and C. Then, the computed optical resistivity values were much lower, $\rho_{op} = (120–260)$ $\mu\Omega$cm, suggesting that the segregation of Si atoms in these films resulted in electrically conductor SiN_x and/or Ta_xSi_y layers instead of an insulating SiNx layer in the grain boundary regions.

Finally, regarding the case of over-stoichiometric films (series C), pure $TaN_{1.14}$ and $Ta_xSi_yN_{0.56}$ films with low Si content exhibited moderate plasma energy values ($\hbar\omega_p = 6$ eV with $N = 2.6 \times 10^{22}\,cm^{-3}$), suggesting that these films contained a higher density of point defects, mainly Ta vacancies and N atoms as antisites.[12] As the Si content increased up to 13 at. %, the spectra can be fitted by decreasing $\hbar\omega_p$ down to 1.5 eV ($N = 1.6 \times 10^{21}\,cm^{-3}$) and increasing Γ_p to 3 eV. The estimated ρ_{op} values were in the range of (350–9915) $\mu\Omega$cm and are compatible to those obtained by van der Pauw measurements. These results suggested that the addition and segregation of Si atoms in over-stoichiometric $TaN_{1.14}$ films lead to the formation of an electrically insulating SiN_x thin layer surrounding the highly defective $TaN_{1.14}$ crystallites. The presence of a high density of Ta vacancies and N atoms in antisite positions, may explain the lower values of the density of free carriers observed in these nanocomposite films with small crystallite sizes.

Downloaded 09 Aug 2013 to 132.248.12.226. This article is copyrighted as indicated in the abstract. Reuse of AIP content is subject to the terms at: http://jap.aip.org/about/rights_and_permissions

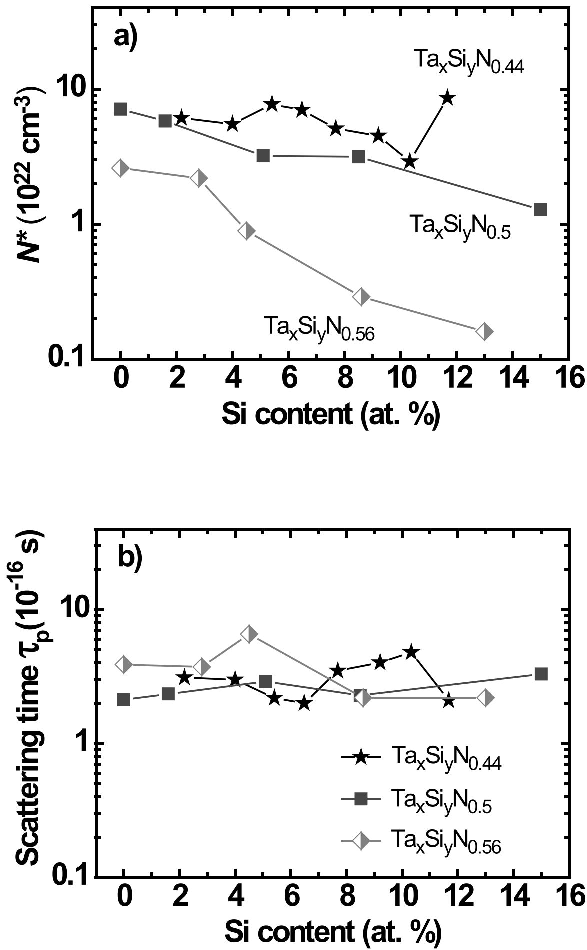

FIG. 6. (a) Charge carrier density and b) scattering time obtained by fitting the data using the Drude-Lorentz model for substoichiometric, near- and over-stoichiometric films.

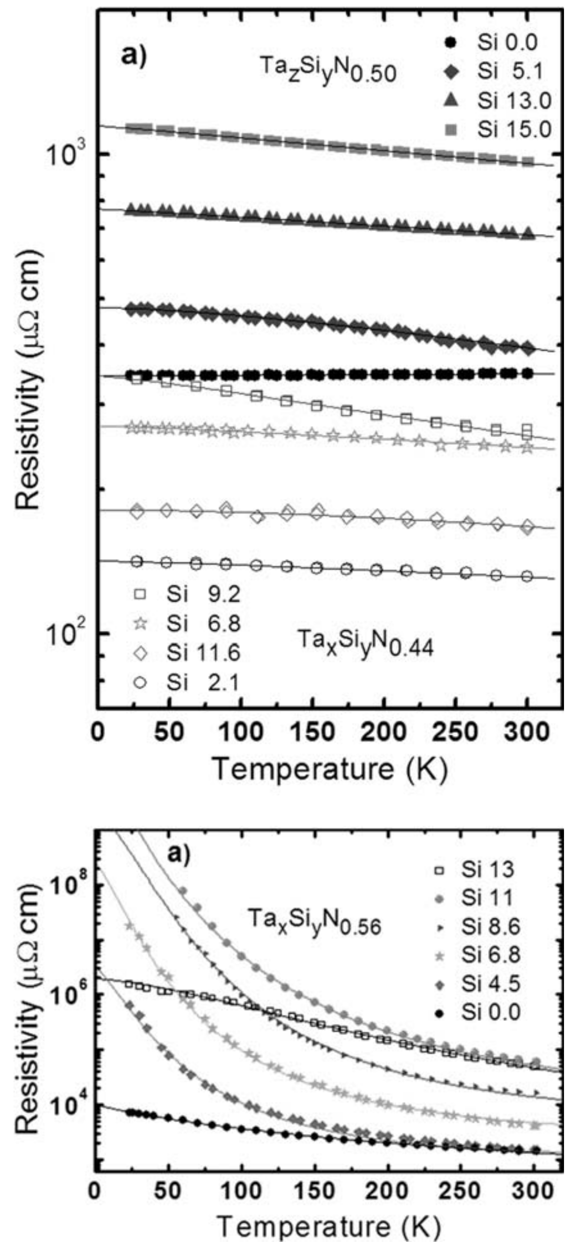

FIG. 7. Temperature-dependent d.c. electrical resistivity $\rho(T)$ curves for selected Si concentrations (in at. %) of: (a) sub-stoichiometric $Ta_xSi_yN_{0.44}$ (open symbols) and near-stoichiometric $Ta_xSi_yN_{0.5}$ thin films (close symbols), b) over-stoichiometric $Ta_xSi_yN_{0.56}$ films. The solid lines are the best fitting with the grain-boundary model.

C. Electrical properties

1. Electrical resistivity

The temperature dependent d.c. electrical resistivity curves of the $Ta_xSi_yN_z$ films for the different Si contents, C_{Si}, are shown in Fig. 7. Sub-stoichiometric $Ta_xSi_yN_{0.44}$ films (series A) exhibited low resistivity values (Fig. 7(a)). The room temperature ρ_{RT} values varied from 140 up to 280 $\mu\Omega$ cm with increasing the Si content. The resistivity of these films exhibited weak temperature dependence with small negative temperature coefficient of resistivity (TCR). In the case of near-stoichiometric $Ta_xSi_yN_{0.5}$ films (series B), ρ_{RT} was directly correlated with the Si content. Stoichiometric TaN films exhibited $\rho_{RT} = 250-350\,\mu\Omega$ cm with slightly positive TCR values. With increasing C_{Si}, negative TCR values were observed and the ρ_{RT} progressively increased up to 960 $\mu\Omega$cm as the C_{Si} is increased up to 13 at. % (Fig. 7(a)). In addition, the over-stoichiometric $Ta_xSi_yN_{0.56}$ films (series C) were characterized by even higher resistivity values and increased negative TCR values. Films with low Si content, $C_{Si} \leq 0.5$ at. %, presented room temperature resistivity ρ_{RT} values of about 950 $\mu\Omega$ cm. Further increase in the Si content lead to a rapid increase in the ρ_{RT} from 1300 $\mu\Omega$ cm for $C_{Si} = 5$ at. % up to $6 \times 10^4\,\mu\Omega$ cm for $C_{Si} = 15.1$ at. % (Fig. 7(b)).

2. Grain boundary model

The transport mechanism in conducting polycrystalline thin films is well described by the grain boundary scattering model.[18–20,36,37] In this model, an effective mean free path $L_G = LG^{(L/D)}$ is introduced to describe the electron scattering including the grain size effect. The inner-crystalline mean free path L, which describes the volume scattering of electrons, is limited by a temperature invariant elastic scattering at lattice defects and acoustic phonons, namely, l_e, and by the temperature dependent inelastic scattering, l_{in}, so that $L^{-1} = l_e^{-1} + l_{in}^{-1}$. The d.c. electrical resistivity is then given by

Downloaded 09 Aug 2013 to 132.248.12.226. This article is copyrighted as indicated in the abstract. Reuse of AIP content is subject to the terms at: http://jap.aip.org/about/rights_and_permissions

$$\rho_g = \rho_B G^{-(L/D)}, \tag{2}$$

where ρ_B is the bulk resistivity, D is the average grain size, L is the inner-crystalline mean free path, and G is the mean probability for electrons to pass a single grain boundary.[36,37] The application of Eq. (2) to the experimental data gives the possibility, by a simple fitting procedure, to obtain pertinent information on the main scattering parameters such as G, D, and l_e and therefore to investigate the influence of the film structure and chemical composition on the electrical properties of the Ta-Si-N films.

By replacing ρ_B in Eq. (2) by the classical expression of the Drude resistivity, the d.c. electrical resistivity is given by

$$\rho_g = \left(\frac{m_e^* v_F}{Ne^2}\right)\left(\frac{1}{L}\right) G^{-(L/D)} = \left(\frac{K}{L}\right) G^{-(L/D)}, \tag{3}$$

where m_e^* is the effective mass of the charge carriers, v_F is the Fermi velocity, and N is the density of the charge carriers. The inelastic mean free path is approximated by $l_{in} \approx \alpha T^{-p}$ where α and p are material specific constants. The theoretical modeling was performed assuming $K = \left(\frac{m_e^* v_F}{Ne^2}\right)$ values according to charge carrier densities N deduced for each sample from the optical measurements and $v_F \approx 10^8\,\mathrm{cm\ s^{-1}}$ and $m_e^* \approx m_e$. Thus, values of $K \approx (50-2300)\ 10^{-7}\ \mu\Omega\,\mathrm{cm}^2$ corresponding to $N \approx (7.0-0.16)\ 10^{22}\,\mathrm{cm}^{-3}$ were used. During the fitting procedure, the N and D values were adjusted to obtain the best fits and the values are shown in Table I. It is worth to mention that the D values obtained by the fitting correspond very well to the grain sizes deduced from glazing incidence diffraction experiments (GI-XRD). The GI-XRD values represent the mean value of the crystallite size at the top surface of the films. So, to a first approximation, these values could be considered as more suitable for calculating electrical parameters, due to the fact that the electrical resistivity is measured in the plane of the film.

The best fits using the model described in Eq. (3) are shown in Fig. 7 as continuous lines for every $Ta_xSi_yN_z$ film. These results indicated that, similarly to earlier reported data for the Nb-Si-N and Zr-Si-N systems,[18,19] the transport mechanism of the $Ta_xSi_yN_z$ thin films can be also described by the grain boundary scattering model. The parameters reported in Table I suggest that, depending on the nitrogen and silicon contents, the transport properties of the $Ta_zSi_yN_x$ films exhibit two different regimes of grain boundary scattering: one regime of moderate electron transmission probability with $0.1 \leq G \leq 0.2$ and another regime of lower probability $G \leq 0.1$ as illustrated in Fig. 8. The former was observed in sub-stoichiometric $Ta_xSi_yN_{0.44}$ regardless of the Si content, and in near-stoichiometric films $Ta_xSi_yN_{0.5}$ with low Si content $C_{Si} < 1.6$ at. %. The latter, $G \leq 0.1$, occurred in $Ta_xSi_yN_{0.5}$ films with $C_{Si} \geq 1.66$ at. % and in all the over-stoichiometric $Ta_xSi_yN_{0.56}$ films.

TABLE I. Typical parameters obtained for the best fit of the electrical resistivity of $Ta_xSi_yN_z$ films using the grain-boundary scattering model as a function of at. % of Si (C_{Si}).

C_{Si} (at. %)	K ($10^{-7}\ \mu\Omega\,\mathrm{cm}^2$)	D (nm)	G	l_e (nm)	α (10^4 nm)	p
Sub-stoichiometric $Ta_xSi_yN_{0.44}$						
2.2	70	4.00	0.18	6	20	1.31
6.8	79	3.97	0.15	6.6	20	1.28
9.2	86	3.95	0.14	6.6	5	1.23
11.6	62	3.80	0.18	6.8	400	1.77
Near-stoichiometric $Ta_xSi_yN_{0.5}$						
0.0	60	2.80	0.140	0.2	1000	2.25
1.6	61	5.86	0.084	9.8	18.7	1.22
3.2	100	4.40	0.081	6.0	40.1	1.52
5.1	116	6.00	0.099	9.1	10.0	1.18
8.5	160	6.00	0.090	9.6	10.0	1.08
15.0	240	6.00	0.090	9.5	7.4	1.10
Over-stoichiometric $Ta_xSi_yN_{0.56}$						
0.0	140	4.80	0.050	10.7	0.30	0.90
2.8	280	4.69	0.048	12.1	0.30	1.13
4.5	450	3.19	0.047	12.7	0.32	1.30
6.8	1000	3.17	0.047	12.2	0.32	1.20
8.6	2000	2.69	0.038	13.5	2.00	1.60
11.0	2000	1.98	0.039	11.8	0.31	1.22
13.0	1000	3.98	0.038	12.6	3.98	1.36

IV. DISCUSSION

In many nanocomoposite nc-MeN/a-SiN_x (Me = Ti, Cr, Zr, Nb) thin films deposited by reactive magnetron sputtering, the electrical and optical properties have been explained in terms of the microstructural modifications of the fcc MeN films due to the addition of Si.[16,18–20] In the case of stoichiometric and over-stoichiometric $Ta_xSi_yN_z$ films (series B and C), the progressive decrease of the crystallize size and the increment of the Si coverage, clearly indicated the formation of a nanocomposite nc-TaN/a-SiN_x with increasing the Si content (see Fig. 1). At C_{Si} of about 4–5 at. %, the TaN crystallites were full covered by 1 ML of SiN_x. Further increase of Si content led to an increase of the Si coverage, e.g., an increase of the SiN_x thickness layer, and further diminution of the crystallite size. However, in the case of sub-stoichiometric films, the structural modifications were different. For Si contents below 6 at. %, the crystallite size slightly decreased while Si coverage increased only up to about 0.4. Between 6 and 8 at. % Si, a sharp increase in the crystallite size up to 12 nm with a similar increase in the Si coverage up to 2.0 was observed. These results suggest that the Si segregation occurs mainly towards the grain boundaries leading to the formation of columnar-needle shaped composite films with a thin a-SiN_x layer between columns rather than an equiaxed nanocomposite film.

The influence of the crystallite size and the presence of the SiN_x layer at the grain boundary regions on the d.c. resistivity (and optical resistivity) were clearly observed in the case of nearly and over-stoichiometric films for the films with Si contents above 4.5 at. %. In both B and C series, the change of the ρ(T) curves from metallic to nonmetallic behavior observed at 4–5 at. % Si (see Fig. 7) can be attributed to the formation of a SiN_x insulating layer around the TaN crystallites. In addition, the optical measurements showed also changes from metallic to dielectric character followed by an important diminution of the free carrier

Downloaded 09 Aug 2013 to 132.248.12.226. This article is copyrighted as indicated in the abstract. Reuse of AIP content is subject to the terms at: http://jap.aip.org/about/rights_and_permissions

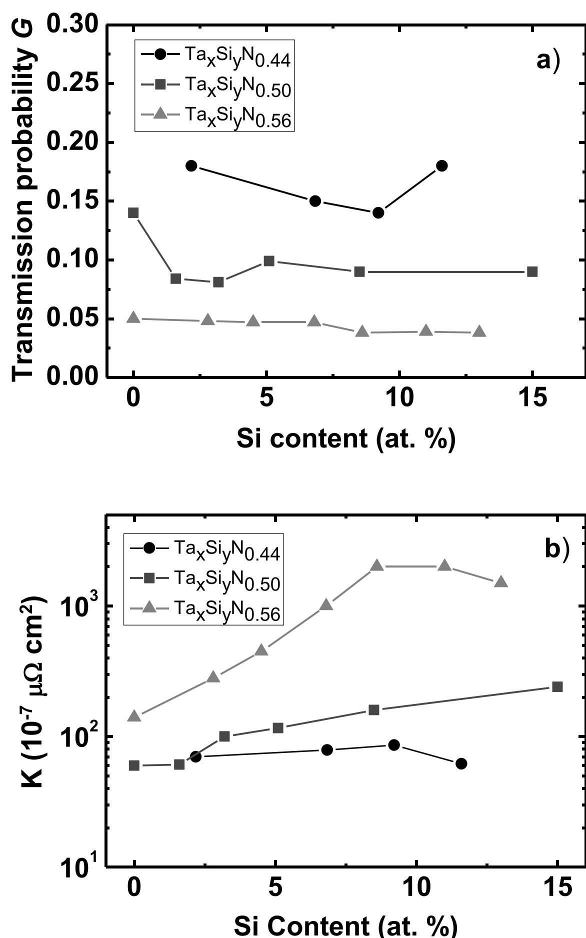

FIG. 8. (a) Grain boundary transmission probability *G* and (b) K values used for the best fitting using the GBS model.

density (see Figs. 3, 4, and 6). The application of the grain-boundary scattering model revealed that the main parameter that controls the transport properties in these films seems to be the presence of a high density of point defects (vacancies and antisites), which can severely decrease the density of the free carries. Both grain boundary regions and point defects contribute to the electrons scattering. The effect of the grain boundaries is noticeable by the diminution of the transmission probability.

On the other hand, in the case of the nitrogen-deficient $Ta_xSi_yN_{0.44}$ films, the resistivity (as well as the free carrier concentration) did not change significantly with increasing the Si content up to 11.7 at. %. The ρ(T) curves were fitted by introducing a grain size of $D \approx 4$ nm and G values of $0.14 \leq G \leq 0.18$. These results clearly indicated that the Si segregation in sub-stoichiometric TaN_x films did not lead to the formation of an efficient electrically insulating SiN_x thin layer probably due to either the low N content in the films or the formation of Ta_ySi_x thin layers at the grain boundaries.[27] Therefore, the weak dependency of the resistivity on C_{Si} for these coatings can be attributed to the frequent percolation of the conducting $TaN_{0.44}$ elongated crystallites separated by conducting SiN_x or Ta_ySi_x thin layers. Similar results have been reported by Jedrzeovski *et al.*[38] for nanocomposite TiN/SiN_x films and, more recently, for ZrN/SiN_x thin films deposited using a bias voltages of -150 V and at substrate temperatures of 510 K and 720 K.[39]

V. CONCLUSION

The optical and electrical properties, as well as the structural variations of $Ta_xSi_yN_z$ thin films deposited by reactive magnetron sputtering were investigated by ellipsometry, d.c. electrical resistivity (van der Pauw configuration) and X-ray diffraction, respectively. The purpose was to investigate the effects of both the N and the Si contents on the structural and opto-electronic properties. For this, three sets of $Ta_xSi_yN_z$ thin films were prepared: sub-stoichiometric $Ta_xSi_yN_{0.44}$, near-stoichiometric $Ta_xSi_yN_{0.5}$, and over-stoichiometric $Ta_xSi_yN_{0.56}$ and for each series, the Si content was varied.

The optical and electrical measurements were interpreted using the extended Drude-Lorentz and the grain boundary scattering models, respectively. The results were consistent indicating that the electronic properties are closely correlated with the compositional and structural modifications of the $Ta_xSi_yN_z$ films and that different trends with the Si content can be obtained depending on the stoichiometry of the TaN_z crystallites. The addition of Si to N-deficient TaN_z samples promoted the formation of columnar-needle shaped composite films with a thin highly nitrogen deficient SiN_x or Ta_ySi_x layer between columns. The sub-stoichiometric $Ta_xSi_yN_{0.44}$ films exhibited metallic properties for all the Si contents. In contrast to that, in the case of nearly stoichiometric TaN or N-rich TaN_z samples, the addition of Si above 4.5 at. % leads to the formation of nanocomposite films with more equiaxed TaN_z nanocrystallites surrounded by an insulating SiN_x layer. The obtained near-stoichiometric $Ta_xSi_yN_{0.5}$, and over-stoichiometric $Ta_xSi_yN_{0.56}$ films exhibited a metal-to-non metal-like transition around 4–5 at. % Si, as observed by both the optical and electrical measurements, in good correlation with the structural changes.

The combination of optical and electrical data gives a complete and coherent description of the evolution of TaSiN films from a solid solution to a nanocomposite material with increasing Si content and stoichiometric variations.

ACKNOWLEDGMENTS

The authors are grateful to the Swiss National Science Foundation and PAPIIT-UNAM 103910 for financial support; G. Ramirez acknowledges the support to CONACYT for Ph.D. scholarship. S.E. Rodil thanks the technical support from H. Zarco for electronic maintenance, A. Tejeda for XRD support and L. Huerta for XPS analysis.

[1] L. E. Toth, *Transition Metal Carbides and Nitrides* (Academic, New York, 1971).
[2] H. Holleck, J. Vac. Sci. Technol. A **4**, 2661 (1986).
[3] A. E. Kaloyeros and E. Eisenbraun, Annu. Rev. Mater. Sci. **30**, 363 (2000).
[4] T. Riekkinen, J. Molarius, T. Laurila, A. Nurmela, I. Suni, and J. K. Kivilauhti, Microelectron. Eng. **64**, 289 (2002).
[5] S. M. Rossnagel, J. Vac. Sci. Technol. B **20**, 2328 (2002).
[6] M. Wittmer, Appl. Phys. Lett. **36**, 456 (1980).
[7] J. M. Daughton, Thin Solid Films **216**, 162 (1992).
[8] X. Sun, E. Kolawa, J. Chen, J. S. Reid, and M. A. Nicolet, Thin Solid Films **236**, 347 (1993).

Downloaded 09 Aug 2013 to 132.248.12.226. This article is copyrighted as indicated in the abstract. Reuse of AIP content is subject to the terms at: http://jap.aip.org/about/rights_and_permissions

[9]T. B. Massalki, in *Binary Alloy Phase Diagrams*, edited by T. B. Massalki (ASM International, Metals Park, OH, 1990), p. 2703.
[10]C. Stampfl and A. J. Freeman, Phys. Rev. B **71**, 024111 (2005).
[11]A. Ishikawa, T. Takata, J. N. Kondo, M. Hara, and K. Domen, J. Phys. Chem. B **108**, 11049 (2004).
[12]C. S. Shin, D. Gall, Y. W. Kim, P. Desjardins, I. Petrov, J. E. Greene, M. Odén, and L. Hultman, J. Appl. Phys. **90**, 2879 (2001).
[13]M. Diserens, J. Patscheider, and F. Lévy, Surf. Coat. Technol. **108–109**, 241 (1998).
[14]J. Musil, Surf. Coat. Technol. **125**, 322 (2000).
[15]S. Veprek, J. Vac. Sci. Technol. A **17**, 2401 (1999).
[16]C. S. Sandu, R. Sanjinés, M. Benkahoul, F. Medjani, and F. Lévy, Surf. Coat. Technol. **201**, 4083 (2006).
[17]E. Martinez, R. Sanjinés, O. Banakh, and F. Lévy, Thin Solid Films **447–448**, 332 (2004).
[18]R. Sanjinés, M. Benkahoul, C. S. Sandu, P. E. Schmid, and F. Lévy, J. Appl. Phys. **98**, 123511 (2005).
[19]C. S. Sandu, F. Medjani, and R. Sanjinés, Rev. Adv. Mater. Sci. **15**, 173 (2007).
[20]C. S. Sandu, S. Harada, R. Sanjinés, and A. Cavaleiro, Surf. Coat. Technol. **204**, 1907 (2010).
[21]J. S. Reid, E. Kolawa, R. P. Ruiz, and M. A. Nicolet, Thin Solid Films **236**, 319 (1993).
[22]D. J. Kim, Y. T. Kim, and J. W. Park, J. Appl. Phys. **82**, 4847 (1997).
[23]Y. J. Lee, B. S. Suh, M. S. Kwom, and C. O. Park, J. Appl. Phys. **85**, 1927 (1999).
[24]Y. S. Suh, G. P. Heuss, and V. Misra, Appl. Phys. Lett. **80**, 1403 (2002).
[25]F. Letendu, M. C. Hugon, B. Agius, I. Vickridge, C. Berthier, and J. M. Lameille, Thin Solid Films **513**, 118 (2006).
[26]J. O. Olowolafe, I. Rau, K. Mr. Unruh, C. P. Swann, Z. S. Jawad, and T. Alford, Thin Solid Films **365**, 19 (2000).
[27]R. Hübner, M. Hecker, N. Mattern, V. Hoffmann, K. Wetzig, H. Heuer, Ch. Wenzel, H. J. Engelmann, D. Gehre, and E. Zschech, Thin Solid Films **500**, 259 (2006).
[28]C. Cabral, Jr., K. L. Saenger, D. E. Kotecki, and J. M. E. Harper, J. Mater. Res. **15**, 194 (2000).
[29]P. Alén, T. Aaltonen, M. Ritala, M. Leskelä, T. Sajavaara, J. Keinonen, J. C. Hooker, and J. W. Maes, J. Electrochem. Soc. **151**, G523 (2004).
[30]K.-M. Jung, M.-S. Jung, Y.-B. Kim, and D.-K. Choi, Thin Solid Films **517**, 3837 (2009).
[31]P. E. Schmid, M. S. Sunaga, and F. Lévy, J. Vac. Sci. Technol. A **16**, 2870 (1998).
[32]R. Lamni, E. Martinez, S. G. Springer, R. Sanjinés, P. E. Schmid, and F. Lévy, Thin Solid Films **447–448**, 316 (2004).
[33]D. Gall, I. Petrov, and E. Greene, J. Appl. Phys. **89**, 401 (2001).
[34]S. M. Aouadi and M. Debessai, J. Vac. Sci. Technol. A **22**, 1975 (2004).
[35]C. Stampfl, W. Mannstadt, R. Asahi, and A. J. Freeman, Phys. Rev. B **63**, 155106 (2001).
[36]A. Nigro, G. Nobile, M. G. Rubino, and R. Vaglio, Phys. Rev. B **37**, 3970 (1988).
[37]G. Reiss, J. Vancea, and H. Hoffman, Phys. Rev. Lett. **56**, 2100 (1986).
[38]P. Jedrzejowski, B. Baloukas, J. E. Klemberg-Sapieha, and L. Martinu, J. Vac. Sci. Technol. A **22**, 725 (2004).
[39]C. S. Sandu, N. Cusnir, D. Oezer, R. Sanjinés, and J. Patscheider, Surf. Coat. Technol. **204**, 969 (2009).

Downloaded 09 Aug 2013 to 132.248.12.226. This article is copyrighted as indicated in the abstract. Reuse of AIP content is subject to the terms at: http://jap.aip.org/about/rights_and_permissions